Results in Engineering 24 (2024) 103201

Contents lists available at ScienceDirect

Results in Engineering

journal homepage: www.sciencedirect.com/journal/results-in-engineering

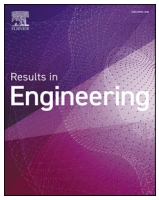

Activated polymeric materials for phosphorus removal in aqueous medium: Study of kinetics and adsorption isotherm

Aydeé Kari-Ferro [a,*], Aydeé M. Solano-Reynoso [b], Celinda Alvarez-Arias [a], Nora Gladis Echegaray-Peña [c], David Choque-Quispe [d]

[a] Agroecological Engineering and Rural Development Departament, Universidad Nacional Micaela Bástidas, Abancay 03001, Perú
[b] Basic Science Department, Universidad Nacional José María Arguedas, Andahuaylas 03701, Perú
[c] Computer Engineering and Systems, Universidad Nacional Micaela Bástidas, Abancay 03001, Perú
[d] Agroindustrial Engineering Department, Universidad Nacional José María Arguedas, Andahuaylas 03701, Perú

ARTICLE INFO

Keywords:
Phosphorus removal
Cellulose nanocrystals
Activated clay
Atomized hydrocolloid
Kinetic models
Adsorption isotherms

ABSTRACT

Excess dissolved phosphorus can cause eutrophication of water bodies. Various porous materials have been proposed to reduce P levels to acceptable levels. The study aimed to evaluate the phosphorus adsorption potential in aqueous media at pH 5, 6, and 8 through citric acid esterified cellulose nanocrystals (NCC), NaCl activated clay (AA), and atomized Nostoc sphaericum hydrocolloid (NS-AH). ζ potential, particle size, zero charge point, total inorganic carbon, TGA, DSC, XRD, and FTIR analysis of the adsorbent materials were determined. The adsorption capacity of P was 16.17, 13.45, and 9.25 mg/g, and removal up to 89.44, 70.35, and 51.66 % by NCC, AA, and NS-AH respectively from 20 ppm P solution. The PFO, PSO, and Intraparticle Diffusion kinetic models were studied, indicating high adsorption rate for AA and NCC during the first 20 min. The study of Langmuir, Freundlich, Redlich-Peterson, Temkin, and Dubinin Radushkevich isotherms showed that the adsorbents present heterogeneous surface, high porosity, and affinity for P at pH 8 in the order NCC > AA > NS-AH and that adsorption is spontaneous and favorable, governing chemisorption processes. The proposed materials, mainly NCC and AA, present high potential for P removal in aqueous media.

1. Introduction

Water bodies, when contaminated with wastewater, especially domestic wastewater, can present a high load of organic matter, and consequently increase carbon, nitrogen, and phosphorus levels. In addition to toxic and recalcitrant substances that alter natural biological processes, making traditional treatments less effective [1].

Phosphorus present in water as soluble orthophosphates, inorganic polyphosphates, and organic phosphates, have as their source detergents, proteins, feces, manure, and urine, which are constituents of wastewater [2]. These, when released into a receiving body without any treatment or poor treatment, damage water bodies [3,4], leading to an increase in nutrients that allow excessive algae development and produce eutrophication [5,6].

Studies have been developed that allow phosphorus to be removed from wastewater through oxidation lagoons, controlled disposal systems in soils, activated sludge, aerobic reactors with biofilm, or combinations of these [7-10]. One of the techniques that allows phosphorus removal in wastewater is through adsorption processes on porous surfaces, which present electrostatic and chemical affinity. These materials can be of biological or inorganic origin, such as clays, agroindustrial residues, native plants, hydrobiological residues, among others [11-15].

Clays have shown considerable interest in the removal of chemicals present in water, such as heavy metals, colored substances, pharmaceuticals, and phosphorus [16,17]. Similarly, materials from vegetable sources and algae show this ability. However, improvements are made to these materials through activation in various media, in order to increase their removal capacity, reaching even nanometer levels [18-20].

However, the use of these materials is limited to the adsorption conditions, such as pH, temperature, and agitation. In addition to the characteristics of the adsorbent materials such as surface area, affinity, active site arrangement, and energy requirement to bind phosphorus or phosphorus forms, which could limit the removal efficiency [10,21,22]. Likewise, the particle size, zeta potential (ζ), crystallinity index, zero charge point, and availability of functional groups influence, are some of the characteristics to take into account when phosphorus adsorption

* Corresponding author.
E-mail address: akari@unamba.edu.pe (A. Kari-Ferro).

https://doi.org/10.1016/j.rineng.2024.103201
Received 12 August 2024; Received in revised form 15 October 2024; Accepted 21 October 2024
Available online 28 October 2024

[23-26].

These characteristics considerably influence the adsorption kinetics. As well as the behavior at different phosphorus concentrations in aqueous media, which is studied through adsorption isotherms. Knowledge of this behavior allows the establishment of operating and treatment conditions [21,27-30].

The adsorption of phosphorus in aqueous media by natural and activated polymers is governed by thermodynamic parameters such as Gibbs free energy (ΔG), enthalpy (ΔH), and entropy (ΔS), which determine the spontaneity and nature of the process [31,32]. Kinetically, the rate constant, equilibrium adsorption capacity, and equilibrium time are critical [31,33]. On the other hand, control parameters such as pH, temperature, and initial adsorbate concentration have a significant influence. The surface area, particle size, zero charge point, zeta potential, and functional groups of the adsorbates are decisive [34,35].

Surface heterogeneity and porosity of adsorbents significantly affect phosphorus adsorption. Heterogeneous surfaces show variations in ΔG° and ΔS°, which affect the spontaneity and disorder of the process [36,37]. While porosity impacts the effective diffusivity, equilibrium adsorption capacity, and adsorption rate. Freundlich, Langmuir, Tempkin, and Dubinin-Radushkevich isotherms and the kinetic models of pseudo-second-order, Elovich, intraparticle diffusion, among others, allow the extraction of parameters that correlate with the surface properties of the adsorbent [33,34,36]. These parameters are determined by adsorption experiments and analyzed by isothermal and kinetic models. Therefore, it is necessary to know and study them before their application on a larger scale

The study aims to show the results and comparison of the physical and chemical characteristics of three activated materials of natural origin such as clay, cellulose from corn husks, and atomized hydrocolloid from the algae Nostoc sphaericum, in the removal of aqueous phosphorus in batches at different pH. The behavior of these adsorbents was also evaluated through the study of the kinetic parameters and adsorption isotherms, as well as the thermodynamic parameters such as Gibbs free energy and adsorption free energy.

2. Materials and methods

2.1. Adsorbent preparation and activation

The clay was treated with 10 % phosphoric acid to remove residual organic matter and rinsed with distilled water to pH 7. It was then activated with 1.0 M NaCl at a ratio of 1/5 (w/w) for 24 h. The solution was sonicated for 3 min (VCX 750 model, Sonic, USA) and rinsed with ultrapure water to 10 μS/cm. It was dried at 60 °C and reduced in size in a planetary mill (PM100 model, Retsch, Germany) to 45 μm, obtaining AA (Fig. 1a).

Algae of the *Nostoc sphaericum* variety were collected from Laguna de Huamanilla, Andahuaylas, Peru, located at 4300 m altitude. The algae were washed with distilled water, removing impurities. It was blended in a 1:1 ratio (w/w) with distilled water. The juice was sieved into a 125 μm mesh and it was atomized at 120 °C inlet temperature, spray gas 650 L/h, aspirator at 85 %, feed rate 5 mL/min, two-fluid nozzle 0.7 mm (Mini Spray Dryer B-290, Büchi, Switzerland), obtaining atomized hydrocolloid (NS-AH) (Fig. 1b).

To obtain NCC, the methodology proposed by [15]. The chopped corn husk (2.5 g) was mixed with a 2 % NaOH solution (50 mL) to remove lignin by microwave digestion for 20 min. The digested sample was brought to neutral pH, then hemicellulose was removed with 0.5 % NaClO for 30 min under stirring and rinsed to neutral pH. The dried samples were microwaved in 3.0 % citric acid solution in a ramp of heating at 160 °C for 15 min and cooling for 10 min, then rinsed to neutral pH and dried at 60 °C and ground to 45 m to obtain NCC (Fig. 1c).

2.2. Zero point of charge (ZCP) and zeta potential (ζ) determination

Solutions with pH 2, 3, 4, 5, 6, 7, 8, 10 and 12 were prepared. 0.05 g of the adsorbent material was added to 50 mL of each solution, and it was stirred continuously at 150 rpm for 24 h at room temperature. At the end, the pH of the resulting solution was measured. The initial and final pH values of each solution were graphed, and the intersection between the curves reported the ZCP value.

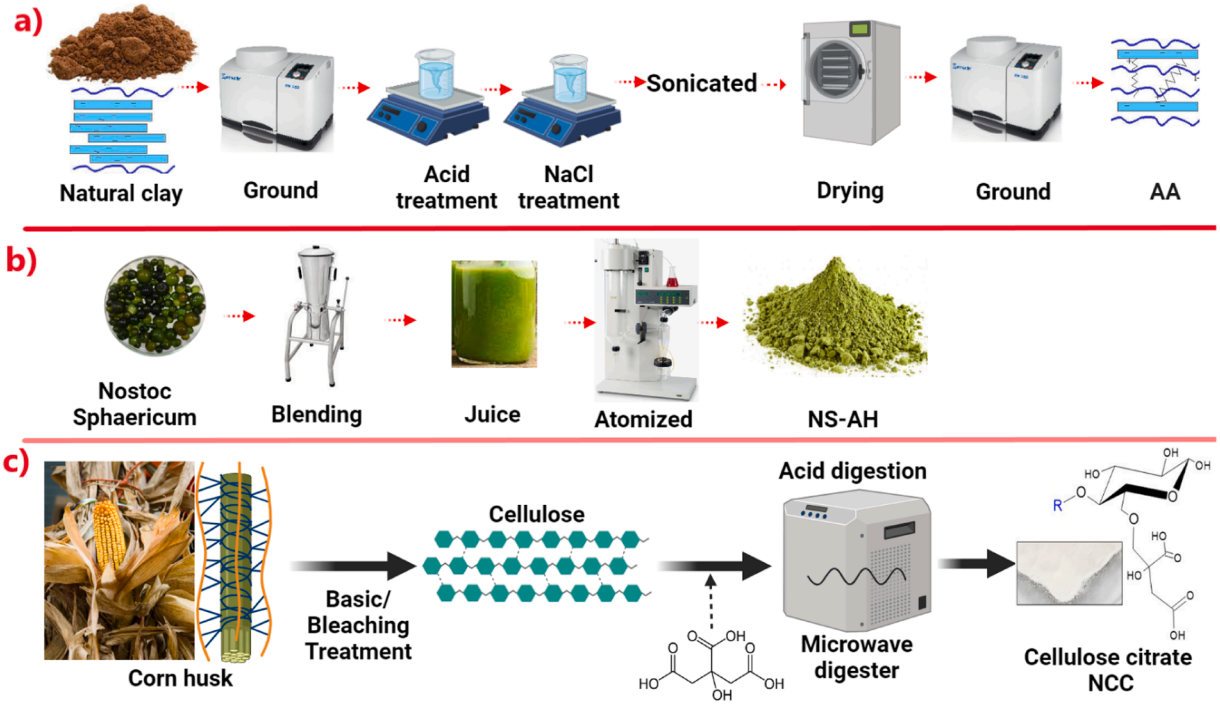

Fig. 1. Obtaining procedure a) for AA, b) for NS-AH, c) for NCC.

The determination of ζ was carried out according to the method proposed by [38], modifying the adsorbent dispersion, which consisted of 4 mg of adsorbent in 50 mL of ultrapure water.

2.3. Total carbon determination

50 mg of adsorbent sample was taken in ceramic crucibles and covered with glass fiber, then taken to the combustion module at 900 °C (TOC-L CSN-SSM 5000A model, Shimadzu, Japan), with an oxygen flow of 150 mL/min. Results were reported in triplicate for total carbon (TC).

2.4. Structural analysis of the adsorbents

The degree of crystallinity (Eq. 1) and the crystal size (Eq. 2) of the adsorbents were calculated from the crystalline phase of the XRD diffractogram. For this purpose, an X-ray diffractometer (D8-Focus model, Bruker, Germany) was used with conditions: Cu Kα1 = 1.5406 A°, 40 kV, 40 mA, and PSD Lynxeye detector [39,40].

$$CD\ (\%) = \frac{S_{cr.p}}{S_t} x100 \tag{1}$$

Where, CD is the crystallinity degree (%); Scr.p is the area corresponding to the crystalline phase; and St is the total area of the diffractogram

$$D = \frac{k.\lambda}{\beta.cos\theta} \tag{2}$$

Where, k is Scherrer's constant (0.9); λ is the wavelength (0.15406 nm); β is the peak width of the diffraction peak profile at half the maximum height resulting from the small crystallite size (rad), θ is the peak position (rad).

The functional groups of the adsorbents, committed to P adsorption, were determined through the transmission-FTIR module (Nicolet IS50, Thermo Fisher, USA), in the scanning range of 4000 to 400 cm^{-1} with 4 cm^{-1} step resolution.

2.5. Thermal analysis of adsorbents

The mass loss as a function of temperature was determined by TGA analysis (STA PT 1600 model, Linseis, Germany) in the range from 20 to 600 °C, with a heating rate of 5 °C/min nitrogen atmosphere. The transition properties of NCC and NS-AH were determined by DSC analysis (DSC2500, TA instrument, USA) with a nitrogen flow of 50 mL/min in the range from 20 to 200 °C at 5 °C/min, following the methodology proposed by [41].

2.6. Determination of phosphorus removal

A solution of 20 mg P/L was prepared with sodium phosphate at pH 5, 6, and 8, subsequently an aliquot was taken. 0.15 g (m) of NCC, AA, and NS-AH adsorbent were placed in 150 mL of P (V) solution under continuous stirring at 120 rpm, for 24 h at room temperature. An aliquot was filtered to 0.45 μm and taken to an ICP OES (9830 model, Shimadzu, Japan). The measurements were carried out in axial mode, flow of 10 L/min of argon gas and 30 s of exposure to plasma. P solutions were prepared at concentrations of 5, 10, 15, 15, 20, 25, and 30 mg/L and a blank with deionized water to construct a calibration curve with an R^2 of 0.995. The removal percentage was determined by the difference in the initial (C_0) and final (C_f) concentration, while the adsorption capacity (q_e) was calculated through Eq. 3 [42,43].

$$q_e = \frac{V(C_0 - C_f)}{m} \tag{3}$$

2.7. Adsorption kinetics assessment

Kinetics describes the adsorption rate of the adsorbate on the adsorbent and determines the time at which equilibrium is reached [44]. The rate of a reaction is defined as the change in the concentration of a reactant or product per unit of time. The reaction order and rate constant are determined by experiments.

Contact times of 0, 30, 60, 90, 120 and 150 min were considered. At the end of each time, an aliquot was filtered at 0.45 microns, and the final P content was determined in an ICP-OES. The study was carried out for each material. With the data obtained, kinetic equations were modeled [45].

The pseudo first order (PFO) model, in its differential form, is proposed through Eq. (4) [46]. The integration for $q_t = 0$ when t = 0 results in Eq. (5).

$$\frac{dq_t}{dt} = k_1(q_e - q_t) \tag{4}$$

$$q_t = q_e(1 - e^{-k_1 t}) \tag{5}$$

Where q_e (mg/g) is the equilibrium adsorption capacity; q_t (mg/g), is the adsorption capacity over time; k_1 is the kinetic constant of the model; t (min) is the contact time.

Although k_1 allows evaluating the speed with which adsorption equilibrium is reached [47], the adsorption rate (PFOrate) is represented through the first term of Eq. 4, so it is more appropriate to calculate through Eq. 6 [48].

$$PPO_{rate} = k_1(q_e - q_t) \tag{6}$$

The pseudo second-order (PSO) model is represented in its integral form through Eq. 7 [49]. For the conditions of $q_t = 0$ when t = 0, Eq. (8) is obtained. Like the PFO model, k_2 measures the rate at which the adsorption equilibrium is reached. However, it is more feasible to measure through the differential term in Eq. 7, so the adsorption rate for the PSO model (PSOrate), can be expressed through Eq. 9 [47,48].

$$\frac{dq_t}{dt} = k_2(q_e - q_t)^2 \tag{7}$$

$$q_t = \frac{q_e^2 k_2 t}{1 + q_e k_2 t} \tag{8}$$

$$PSO_{rate} = k_1(q_e - q_t)^2 \tag{9}$$

Where, $k_2(g/mg.min)$ is the kinetic constant of the model.

The intraparticle diffusion (ID) model (Eq. 10), is formulated on the basis that the adsorption process can be controlled by several stages, including diffusion within the adsorbent, sorbate diffuses from a high concentration zone to the surface and within the adsorbate to the active sites (intraparticle diffusion) [31].

$$q_t = k_i t^{1/2} + C \tag{10}$$

Where k_i is the intraparticle diffusion rate (mg/g.$min^{1/2}$), C is the constant relating the average thickness of the boundary layer (mg/g).

If $C = 0$, adsorption at the surface is negligible, and intraparticle diffusion completely controls the adsorption process. If $C \neq 0$, the adsorption process happens at the surface and intraparticle level. High C values indicate that the adsorption process is preferentially superficial [31,33].

2.8. Adsorption isotherm assessment

Equilibrium data can be tested with some isotherm models such as Langmuir, Freundlich, Tempkin, Dubinin-Raduskevich, these isotherms allow describing adsorption processes [50].

The Langmuir model (Eq. 11) considers the homogeneous surface of the adsorbent and allows representing the adsorption for multi-metallic

systems on the active sites at the monolayer level [49,51]. The affinity of the adsorbent material for the adsorbate was measured by the separation factor R_L (Eq. 12), if RL > 1.0 the process is unfavorable, $0 < R_L < 1.0$ is favorable and $R_L = 0$ is irreversible.

$$q_e = \frac{q_m k_L C_e}{1 + k_L C_e} \tag{11}$$

$$R_L = \frac{1}{(1 + k_L C_0)} \tag{12}$$

Where, $q_e(mg/g)$ is the equilibrium adsorption capacity; $k_L(L/mg)$ is the Langmuir constant; $C_e(mg/L)$ is the adsorbate concentration at equilibrium; $q_m(mg/g)$ is the adsorption capacity in the monolayer.

The Freundlich model (Eq. 13), considers a heterogeneous adsorption surface (ideal), with different adsorption energies and reversible [49,52].

$$q_e = k_f C_e^{1/n} \tag{13}$$

Where, K_f ($mg^{1\text{-}1/n}/L^n$) and n are Freundlich's constants, adsorption capacity and adsorption intensity indicators respectively.

The Redlich-Peterson isotherm (Eq. 14) is a more flexible model that explains adsorption on heterogeneous and multilayer surfaces, with distribution of active sites of different energy and pores of different sizes [53].

$$q_e = \frac{k_R C_e}{1 + a_R C_e^g} \tag{14}$$

Where, k_R (L/g) is the parameter that indicates the maximum adsorption capacity; a_R $(L/mg)^g$ model parameter, high values indicate greater saturation; g is the parameter that varies between 0 and 1. When $g = 1$, it reduces to the Langmuir isotherm, and when $g \neq 1$ it represents a combination of the Langmuir and Freundlich isotherms

The Tempkim model (Eq. 15), allows to know the variation of the adsorption energy of the adsorbent-adsorbate interaction, and that it decreases linearly in multilayers [54,55]

$$q_e = \frac{RT}{b_t} \ln(A_t C_e) \tag{15}$$

Where, R is the universal ideal gas constant (8.314 J/mol.K); T is the absolute temperature (K); b_t(J/mol) is the variation of adsorption energy; A_t (L/mg) is the equilibrium bonding constant corresponding to the maximum bond.

The Dubinin and Radushkevich isotherm (Eq. 16), allows to represent the free energy of adsorption at sites of varying porosity (high degree of rectangularity), being able to know if the process is physical or chemical for heterogeneous systems [51,56].

$$q_e = q_D \exp\left(-B\varepsilon^2\right) \tag{16}$$

Where, q_D (mg/g) is the theoretical saturation capacity; B $(mMol^2/J^2)$ is the constant related to the mean free energy of adsorption E (Eq. 17); ε is the Polanyi potential, which is related to the equilibrium according to Eq. (18).

$$E = 1/(2B)^{1/2} \tag{17}$$

$$\varepsilon = RT \ln(1 + 1/C_e) \tag{18}$$

The values of E allow to know if the adsorption is physical or chemical. If $E < 8$ kJ/mol the adsorption is physical, if $E > 8$ kJ/mol the adsorption is chemical.

The isotherm and kinetic models were fitted by nonlinear regression, with the criterion being the least squares difference, evaluated by the Quasi-Newton method [57]. The adjustment was performed by error functions such as the adjustment coefficient R^2 which measures the variability of the dependent variable of the adjusted model. The relative average error (*ARE*) which minimizes the fractional error distribution, and the Chi-square test (X^2) reports the smallest difference between the experimental and fitted values. The hybrid fractional error function (HYBRID). The Marquardt percentage deviation function (MPSD) measures the geometric mean error distribution [58,59].

$$ARE = \frac{100}{N} \sum_{i=1}^{N} \left| \frac{q_{adj} - q_{exp}}{q_{exp}} \right|_i \tag{19}$$

$$X^2 = \sum_{i=1}^{N} \left[\frac{\left(q_{exp} - q_{adj}\right)^2}{q_{adj}} \right]_i \tag{20}$$

$$HYBRID = \frac{100}{N - n} \sum_{i=1}^{N} \left[\frac{\left(q_{adj} - q_{exp}\right)^2}{q_{exp}} \right]_i \tag{21}$$

$$MPSD = 100 \sqrt{\frac{1}{N - n} \sum_{i=1}^{N} \left[\frac{\left(q_{adj} - q_{exp}\right)^2}{q_{exp}} \right]_i} \tag{22}$$

Where q_{adj} is the adsorption capacity reported by the model; q_{exp} is the experimental adsorption capacity; N corresponds to the number of data, and n is the number of model parameters.

R^2 values close to unity indicate good model fit, while *ARE*, X^2, *HYBRID*, and *MPSD* should be as low as possible [60,61].

The data analysis was carried out with a significance level of 5 %, with the help of Excel sheets, solver utility, Statistica V12, and Origin Pro 2022 software.

3. Results and discussion

3.1. Adsorbent characteristics

The pH in the ZCP was observed to be 5.10 for NCC, 6.00 for AA, and 9.10 for NS-AH (Table 1). The adsorbents NCC and AA have a net positive surface charge, which would give them a higher affinity for anions, while NS-AH has a low affinity, although it is more stable to pH changes (Fig. 2a). This affinity would be subject to other factors such as the adsorption temperature, the ionic strength of the solvent medium, the competition or presence of ions that are not adsorbed, and the contact time, which could produce reversibility in the adsorbent-adsorbate complex [62-64].

The adsorbent materials studied are at the nanometer level, with values ranging from 22.10 to 648.70 nm for NS-AH, 65.00 to 487.50 nm for AA, and 676.90 nm for NCC (Table 1). These sizes would allow them a high contact area, shorter adsorption time improving their kinetics, and less amount of adsorbent [65,66].

The ζ of the materials are high in their absolute value, 24.67 mV for NCC, 28.96 mV for NS-AH, and 39.91 mV for AA (Table 1), these values suggest that the materials are stable to sedimentation, with low aggregation. When they are used in an aqueous medium, with a considerable residence time in suspension, giving it the necessary time to be able to adsorb other constituents on its surface [67-69].

Regarding TOC, AA presented low values (0.34 %), this is due to the fact that they could host some organic material in their porous structure. NCC and NS-AH reported high TOC values of 49.14 and 40.67 % respectively (Table 1), these values are due to their constitution, mainly of glucose and protein carbon chains. On the other hand, no inorganic carbon was identified in any of the materials.

The study of X-ray diffraction allows to know the structural arrangement and composition of the materials, as well as the spatial disposition of atoms and molecules [70,71].

It was observed that AA presents characteristic Riebeckite and Albite peaks. While NCC and NS-AH presented a type B diffraction pattern (Fig. 2d) due to the presence of characteristic peaks of higher intensity at 2 θ around 20°, which correspond to double helices with a hexagonal

Table 1
Adsorbent characteristics.

Adsorbent	Size (nm)*			ζ (mV)	pH_{ZCP}	TOC (%)		Crystallinity index (%)	Crystal size (nm)	
	Peak	$\bar{x}$	%			$\bar{x}$	±s		$\bar{x}$	±s
AA	1	65.00	2.60	-39.91	6.00	0.34	0.01	50.39	52.16	33.03
	2	487.50	97.40							
NCC	1	676.90	100.0	-24.67	5.10	49.14	0.94	72.94	0.77	0.05
NS-AH	1	22.10	1.30	-28.96	9.10	40.67	0.16	80.00	0.81	0.14
	2	121.60	15.10							
	3	648.70	83.60							

Where $\bar{x}$, is the arithmetic mean; s, is the standard deviation; ζ, zeta potential; pH_{ZCP}, pH at zero loading point; TOC, is total organic carbon.
* Evaluated through NICOMP distribution.

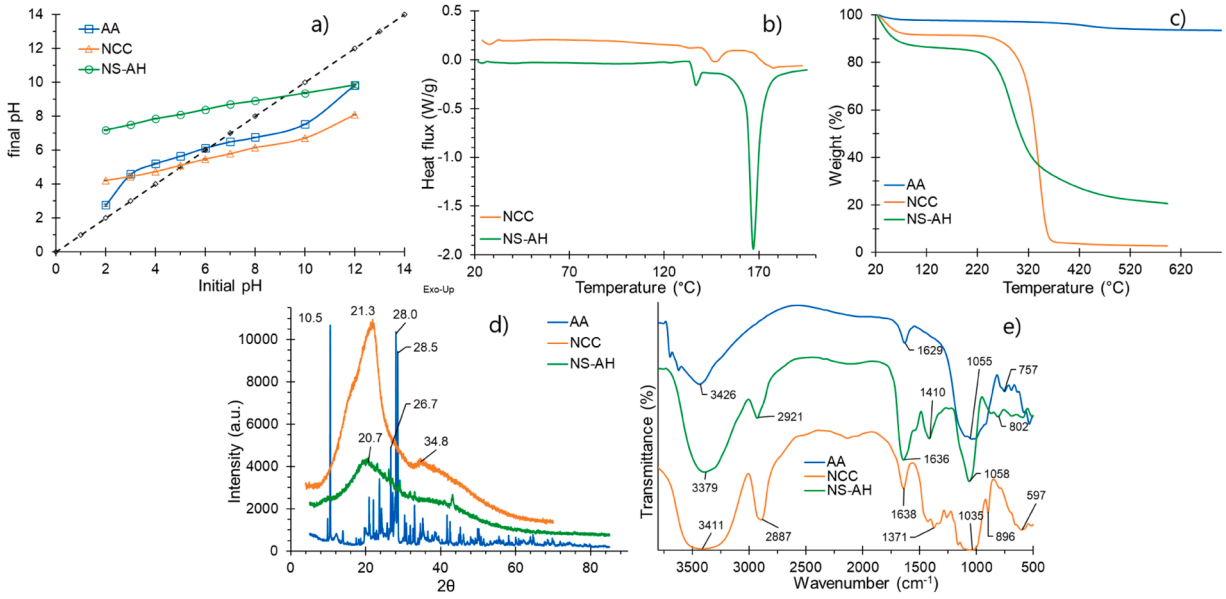

Fig. 2. Adsorbent characteristics, a) ZCP, b) TGA thermograms, c) DSC thermograms, d) XRD diffractogram, e) FTIR spectrogram.

arrangement and with the presence in its structure of 36 water molecules, this characteristic is typical of starches, carbohydrates, gums and hydrocolloids [72-74].

On the other hand, it was observed that the crystallinity index was reported in the order NS-AH > NCC > AA (Table 1). This would indicate that NS-AH (IC 80.00 %) would present better ordering of its crystalline networks with lower specific surface area, giving it lower porosity and active sites to bind molecules, with a high probability of occurrence of physisorption processes. On the contrary, NCC and AA would present a more heterogeneous surface with high porosity with surface defects, so chemisorption processes would predominate in these materials [75].

FTIR analysis allows for identifying the functional groups of the adsorbents and knowing the stretching, bending, and torsion-type interactions of the chemical bonds in the materials [15,76]. High-intensity peaks were observed around 3400 cm^{-1} in the three materials (Fig. 2e), this would correspond to the stretching of the hydroxyl groups of the S-OH arrangement and water in AA, while for NS-AH it would correspond to water, amides, carbohydrates, and carboxylic acids. For NCC it would be due to water and carbohydrates. Around 2900 cm^{-1} high-intensity peaks are observed for NCC and NS-AH, this would be due to the C-H vibrations of the methyl groups of the carbohydrates, which is characteristic of materials of biological origin [77], observing that AA is not present.

Regarding the peak around 1600 cm^{-1}, it would be attributed to the -OH stretching of adsorbed water molecules [78,79], with greater intensity for NS-AH (Fig. 2e), which suggests a highly hygroscopic material, due to its hydrocolloid content [80,81]. The peak at 1410 cm^{-1} in NS-AH and 1371 cm^{-1} for NCC is due to stretching of the C-O, C-H, and -OH single bonds, mainly of the carbohydrates.

On the other hand, the peak around 1050 cm^{-1} corresponds to the stretching of the C-O, C-O-C, and C-OH bonds of the polymer chains in NCC and NS-AH [82,83]; while in AA it is due to Si-O stretching (out of plane) [84,85]. The peaks below 1000 cm^{-1} correspond to the fingerprint of the materials, which in the case of NCC and NS-AH are attributed to stretching of the C-H and C-O bonds, belonging to starches and glucose, which is characteristic of hydrocolloids and cellulosic material [82,86,87]. While for AA it would be related to Al-O-Si deformation, and Si-O-Mg and Si-O-Fe vibration bending [88,89].

The thermal behavior of the NCC and NS-AH materials was evaluated through a DSC analysis. The presence of a small peak was observed that would correspond to the glass transition temperature (T_g) at 148 °C for NCC and 137 °C for NS-AH, in the same way, a high-intensity peak was observed for NS-AH, which would correspond to the melting temperature (T_m) at 167 °C, while for NCC the peak is slight and occurs at 178 °C (Table 2).

The fact that T_m is intense for NS-AH (Fig. 2b), is due to the presence of carbohydrates, gums, and some proteins [15,90], these constituents of

Table 2
DSC thermal transitions for the adsorbents.

Adsorbente	T_g (°C)	ΔH (J/g)	T_m (°C)	ΔH (J/g)
NCC	148	0.91	167	11.91
NS-AH	137	1.67	167	230.16

the materials generally report high values, due to their nature. While for NCC it is not observed, because it is constituted only of cellulose crystals, which do not show melting behavior [91].

Where, Tg is the glass transition temperature; Tm is the melting temperature; ΔH is the enthalpy change.

To know the mass variation as a function of temperature increase, a TGA analysis was carried out. Three stages were observed for the three adsorbents. The first stage corresponds mainly to water loss, with NS-AH reporting 11.29 %, while AA reported only 4.94 % (Table 3). This difference is mainly due to the presence of hygroscopic functional groups such as carbonyls, hydroxyl, and carboxyls in NS-AH and NCC [92], which have a high capacity to bind water through hydrogen bonds. While, the silicate and aluminate groups of AA have a low willingness to trap water [79], although this occurs up to 163.98 °C due to interlaminar water[93].

The second stage (Fig. 2c) corresponds to weight loss due to the decomposition of low molecular weight carbohydrates in NCC and NS-AH, which occur at lower temperatures compared to AA. This difference is due to the fact that for AA, in that temperature range (163.98 to 630.73 °C) the reorganization of its structure occurs, allowing the elimination by volatilization of free aluminum [94].

In the third stage, mass loss is manifested due to the decomposition of the organic matter of NCC and NS-AH with residual carbon and mineral content, which occurs around 600 °C. While for AA, the structural water loss of the hydrated material would reach 0.265 %, which is characteristic of these materials [93-95].

The study of the thermal stability and structural integrity of the adsorbents studied and analyzed by TGA, DSC, XRD, and FTIR are critical for their long-term usefulness and their contribution to the circular economy. A high thermal stability allows the adsorbent to be resistant in wide temperature ranges, facilitating efficient regeneration cycles. This condition is favored for AA, while the opposite is true for NCC, although the operating temperatures would condition it.

On the other hand, a stable crystalline structure indicates greater resistance to chemical and mechanical degradation, prolonging its useful life and maintaining its efficiency after regeneration [70,75,96], so NCC, AA, and NS-AH would be favored. These factors, in addition to surface area, porosity, and presence of functional groups, determine the viability, durability, and efficiency of the adsorbents studied for the adsorption of phosphate species, which would increase their reuse cycle. However, it is necessary to consider real scenarios to verify this [97].

3.2. Phosphorus removal

It was observed that NCC reported greater phosphorus removal in the form of phosphate ion, reaching 89.44 % and 16.17 mg P/g, followed by AA with values between 60.53 and 70.35 %. In comparison, NS-AH reported removal between 47.24 and 51.66 % (Table 4), showing significant differences with the pH of the aqueous medium. The reported values are encouraging for the materials studied compared to other materials used, where doses of adsorbents and phosphorus concentrations similar to the present study are applied, with slightly identical results (Table 4).

Iron oxides and activated carbon are more effective in removing phosphorus from aqueous media (Table 4). Iron oxides offer high adsorption capacity, are regenerable, and effective over a range of pH, but can be expensive and release iron into the water. Carbon materials, on the other hand, have a high specific surface area and can be produced from waste, but this process is expensive and can leave harmful residues in the water [98-103]. Thus, cellulose is an economical, biodegradable, and chemically modifiable material. Similarly, clays offer a balance between cost and efficiency, being cheaper and more abundant than iron oxides and activated carbon, but less efficient, although with better results than cellulose and hydrocolloids. The choice of adsorbent material depends on the balance between efficiency, cost, and environmental considerations.

However, the adsorption capacity is affected by the presence of competing anions such as sulfate, nitrate or chloride when treating real wastewater. These anions compete directly for adsorption sites with preference given to polyanionic ions, although the pH of the medium influences these interactions, with greater interaction at lower ZCP values [98,104,105], which could slow down the kinetics, diffusivity and cation exchange of AA, NCC, and NS-AH adsorption.

The esterification of NCC forms cellulose citrate, which increases the number of oxydryl groups, giving it the ability to form hydrogen bridge bonds [108,109]. Activation of the clay with NaCl improves the ion exchange capacity [110], which would facilitate the adsorption of phosphate ion species. Although they are subject to variations in the pH of the aqueous medium and the ζ potential of the material, they are usually activated with different chemicals or methods [111,112]. In NS-AH, the adsorption capacity is due to the chelating groups they present, mainly formed by proteins and carbohydrates, although these do not show good affinity. The fact that NCC has a higher affinity for phosphates is due to the ester group and its polarity [113].

Phosphate-derived species or ions have preferences during adsorption. At pH 5, the $H_2PO_4^{1-}$ ion predominates (Fig. 3a), which has a higher affinity for the adsorbent materials due to electrostatic attraction with the positively charged active sites of the materials [4,100,114-116], mainly the NCC, as evidenced by FTIR analysis (Fig. 2c).

With increasing pH, the number of electrical charges of phosphate (PO_4^{3-}) is higher (Fig. 2a), and this species requires more binding energy for adsorption, which decreases the adsorption capacity due to increased electrostatic repulsion with the negatively charged sites of the materials [100,114]. This is because they are at or beyond the cationic zone established by the ZCP (Fig. 2a), where there is a preference for positively charged species at alkaline pH.

This behavior is characteristic of phosphorus removal in the form of phosphates [102,117-120]. However, the formation of phosphate salts is promoted at basic pH, which would be reflected in a decrease of phosphates and their species in aqueous media, improving their removal (Fig. 3a) [3,4,107]. The pH range to improve adsorption depends on the characteristics and preparation of the materials, such as impregnation with metal oxides, surfactants, bases, and strong acids [19,107,116,121].

AA, NCC, and NS-AH have nanometric sizes that allow for greater adsorption capacity due to the increased availability of contact area between the adsorbent and adsorbate. This conformation allows the availability of electrical charges on the material's surface, which improves the strength of the interaction between the adsorbent and the adsorbate. This is evidenced by the values found for the potential ζ for the studied materials [69,121].

Table 3
Weight loss from TGA analysis for adsorbents.

	1st stage		2nd stage		3rd stage		Residue (%)	Maximum weight loss (%)
	Weightloss (%)	Temp, (°C)	Weightloss (%)	Temp, (°C)	Weightloss (%)	Temp, (°C)		
AA	4.94	163.98	6.05	630.73	0.265	993.29	88.741	11.259
NCC	7.71	72.05	87.56	367.90	1.926	593.7	2.804	97.196
NS-AH	11.29	67.25	47.41	323.02	20.6	590.1	20.7	79.3

Table 4
Adsorption capacity and phosphorus removal.

	Material	pH	q_e (mg P/g)			Removal (%)				Adsorbed ion
			$\bar{x}$	±s	CV	$\bar{x}$	±s	CV	*	
T1	AA	5	11.27	0.15	1.33	60.53	0.18	0.29	a	PO_4^{3-}/$H_2PO_4^{1-}$
T2	AA	6	12.13	0.15	1.27	63.97	0.15	0.24	b	$H_2PO_4^{1-}$/ PO_4^{3-}
T3	AA	8	13.45	0.16	1.21	70.35	0.35	0.50	c	$H_2PO_4^{1-}$/ HPO_4^{2-}
T4	NS-AH	5	8.50	0.13	1.54	47.24	0.68	1.44	d	PO_4^{3-}/$H_2PO_4^{1-}$
T5	NS-AH	6	8.91	0.25	2.81	49.51	0.63	1.28	e	$H_2PO_4^{1-}$/ PO_4^{3-}
T6	NS-AH	8	9.25	0.36	3.85	51.66	0.85	1.65	f	$H_2PO_4^{1-}$/ HPO_4^{2-}
T7	NCC	5	12.87	0.25	1.94	74.14	0.58	0.78	g	PO_4^{3-}/$H_2PO_4^{1-}$
T8	NCC	6	14.57	0.26	1.77	80.66	0.44	0.54	h	$H_2PO_4^{1-}$/ PO_4^{3-}
T9	NCC	8	16.17	0.28	1.72	89.44	0.09	0.10	i	$H_2PO_4^{1-}$/ HPO_4^{2-}
Deng and Shi [24]	Mesoporous modified kaolin clay (MKC)	7.5				98.03				AD: 4 g/L, IC: 25 ppm
Cui et al. [101]	Fe3O4 and the Mg–Al layered double hydroxide	3.0–11.0	82.46							AD: 1 g/L, IC: 50 ppm
Yin et al. [106]	Calcium-rich sepiolite (NOCS)	3.0–6.0	32.00							AD: 20 g/L, IC: 5 to 800 ppm
Jung et al. [102]	novel magnesium ferrite (MgFe2O4)/biochar magnetic composites	3.0	53.16			80.40				AD: 0.2 g/L, IC: 100 ppm
Wang and Sun [4]	Fly ash with medium calcium content	5.5	7.97							AD: 6.0 g/L, IC: 10 ppm
Chen et al. [16]	thermally treated bentonite	3.0–11.0	6.94			94.00				AD: 20 g/L, IC: 10 - 100 ppm
Sun et al. [18]	Shell Powder	8.0				≈ 90.00				AD: 11.40 g/L, IC: 9.8 ppm
Ding et al. [27]	MIEX resin					≈ 97.00				AD: 1.0 mL/L, IC: 15.0 ppm
Wang et al. c	Rare earth element doped magnetic biochars	6.5	63.0							AD: 0.5 g/L, IC: 50.0 ppm
Xanthopoulou et al. [107]	Polyethylenimine Functionalized Silica-Based Materials	5.0				80.0				AD: 0.1 g/L, IC: 1.0 ppm
Shumiye et al. [103]	Sludge carbon	3.0				83.4				AD: 3.0 g/L, IC: 30.0 ppm
Hu et al. [100]	Hierarchical CuAl/biomass carbon fiber layered double hydroxide	8.0				99.6				AD: 0.2 g/L, IC: 50.0 ppm
Jia et al. [99]	Porous honeycomb cork biochar	3-10				<99.0				AD: 0.5 g/L, IC: 20.0 ppm
Santos et al. [104]	biogenic calcium carbonate	7.33		4.57						AD: 20.0 g/L, IC: 40.0 ppm
Ramirez et a. [105]	Aluminum-doped ferrite raspberry-shaped nanostructures	3.0		15.5						AD: 1.0 g/L, IC: 50.0 ppm
Jung et al. [98]	Lepidocrocite	7.4				91.5				AD: 40.0 g/L, IC: 10.0 ppm

Where, $\bar{x}$ is the arithmetic mean; s is the standard deviation; AD is adsorbent dose; IC is initial concentration of P.

3.3. Phosphorus adsorption kinetics

The pseudo-first order (PFO) model reported higher q_e values for NCC, with values up to 17.7294 mg/g, for AA 12.2434 mg/g, and NS-AH 9.9646 mg/g. The pseudo-second order (PSO) model was slightly higher (Table 5). This difference is due to the limitations of both models. PFO assumes that maximum adsorption occurs at the monolayer level with the same energy level over the entire adsorbent surface and that the rate of active site occupation is proportional to the number of unoccupied sites on the adsorbent. While PSO, in addition to the above mentioned for PPO, considers that adsorption happens by chemisorption, presenting strong interactions, and that the occupation rate of adsorption sites is proportional to the square of the number of active sites in the adsorbent [120,122-124].

NCC esterified in citric acid has -$COOH^+$ groups that have been protonated by the H^+ of citric acid, forming positively charged ester groups [125,126], which facilitates the chemisorption of phosphate and its species.

On the other hand, AA, when activated with NaCl (sodification process), acquires a lower hydration energy, resulting in Na^+ ions on the surface of the clay (AA), resulting in a higher positive charge density [127-129]. This favors the attraction of negatively charged ions such as phosphates and their anions. Whereas in NS-AH, the groups responsible for trapping phosphate ions are the amino groups and derivatives of demethylated galacturonic acid [124,130,131].

The $H_2PO_4^{1-}$ ion predominates at pH values above 2.0 (Fig. 3a) and dissociates up to 99.9 % at pH 7.0, so this species has more affinity to bind to the positively charged active sites of the adsorbent. Added to this is the fact that the dissociation of the HPO_4^{2-} and PO_4^{3-} species is very low compared to the first ion [14,132,133]. This is evident when it is appreciated that as the pH of the adsorption system increases for the three adsorbents, the value of q_e increases significantly (Table 5), and this is confirmed with the ZCP of the adsorbents.

The adsorption rate K_1 values for PFO showed higher values for AA, indicating that the adsorption of phosphate and its species was faster in this material, followed by NCC and NS-AH. The same trend was observed for the K_2 constant for the PSO model (Table 5).

The fitted curves for phosphate adsorption kinetics (Fig. 3b) show rapid adsorption during the first 20 min, reaching equilibrium around 30 min. The initial adsorption rate h of PSO increases significantly with

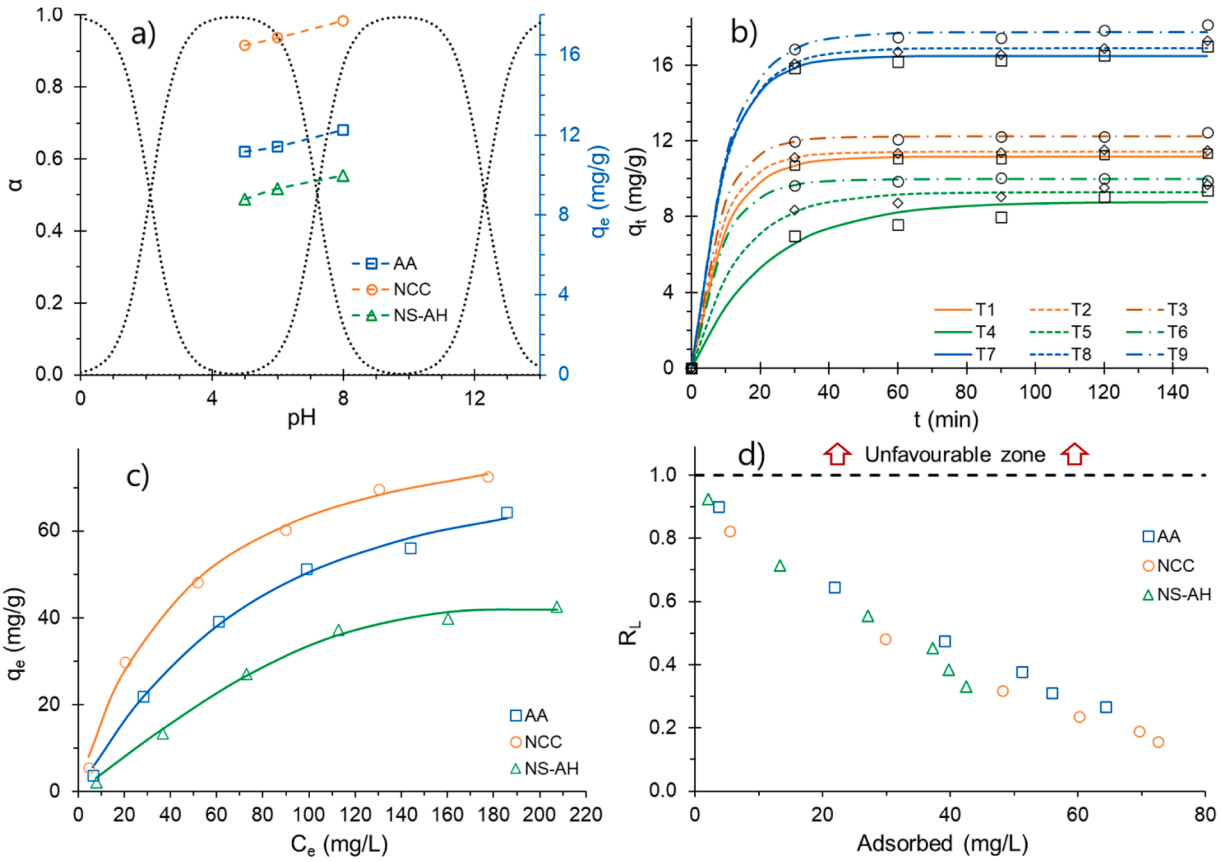

Fig. 3. a) Phosphate species distribution and adsorption capacity, b) Kinetic curves of phosphorus adsorption, c) Adsorption isotherm for phosphorus, d) Behavior of RL separation factor for the adsorbents.

Table 5
Kinetic model parameters.

	Adsorbed	pH	PFO			PSO				DI	
			q_e (mg/g)	K_1 (min^{-1})	rate*	q_e (mg/g)	K_2 (g/mg.min)	h (mg/g.min)	rate**	K_{di} ($mg/g.min^{1/2}$)	C (mg/g)
T1	AA	5	11.1723	0.1047	0.0506	11.4157	0.0423	5.5187	0.0230	0.8842	2.4602
T2	AA	6	11.4264	0.1181	0.0390	11.5878	0.0645	8.6634	0.0158	0.8973	2.5989
T3	AA	8	12.2434	0.1262	0.0350	12.4097	0.0665	10.2461	0.0154	0.9635	2.7827
T4	NH	5	8.7719	0.0460	0.1015	9.8896	0.0069	0.6780	0.0726	0.7418	1.1514
T5	NH	6	9.2986	0.0719	0.0773	9.8747	0.0165	1.6091	0.0464	0.7613	1.7220
T6	NH	8	9.9646	0.1141	0.0371	10.1007	0.0727	7.4213	0.0140	0.7802	2.2780
T7	NCC	5	16.4829	0.1075	0.0704	16.8714	0.0278	7.9004	0.0349	1.3110	3.5906
T8	NCC	6	16.8639	0.1006	0.0829	17.2772	0.0247	7.3820	0.0387	1.3387	3.6651
T9	NCC	8	17.7294	0.0983	0.0913	18.2067	0.0215	7.1130	0.0440	1.4105	3.8182

increasing pH, reaching 10.2461 mg/g.min for AA and 7.4213 mg/g.min for NS-AH. This suggests the presence of a greater number of positively charged active sites on the surface of these materials at high pH, whereas for NCC the initial adsorption rate is similar in both acidic and alkaline media (Table 5). On the other hand, the adsorption rate PFOrate and PSOrate at 30 min, presented inverse values to *h*, this indicates that adsorption would occur in the remaining sites and intraparticle or intraporous adsorption would occur, which is characterized by being slower. The opposite happens for NCC, this would be due to the slow availability of active centers with positive charge, due to the low hydration of this material.

The intraparticle diffusivity model allows to know the adsorption phenomenon inside the pores of the studied materials and could relate to the porosity of the materials [28,134], although its parameters lack a physical or thermodynamic definition.

It was observed that the intraparticle diffusion rate, K_{di}, increases significantly with pH and is in the order of NCC > AA > NS-AH (Table 5). The C values obtained indicate that the adsorption process takes place at the surface and intraparticle levels. Lower values were observed for NS-AH, suggesting that this material could have a higher porosity, whereas NCC would have a lower porosity, as high values of C indicate that the adsorption process is preferentially superficial [28,31,33].

R^2 values > 0.97 were observed for the PFO and PSO models (Table 6), indicating a good fit, although this parameter has some limitations, especially in the number of points or data evaluated. It is also advisable to use other statistics such as X^2, whose low values indicate a good fit [123,135], as found for the models studied for the three adsorbents studied.

The adsorption kinetics depends on the rate of diffusion of phosphate ions towards the surface of the adsorbents; high values of the potential ζ (in absolute value) generate a stronger electric field around the adsorbents. This effect is enhanced when the adsorbent particles are small

Table 6
Fit statisticians for kinetic models.

Model	Statisticians	T1	T2	T3	T4	T5	T6	T7	T8	T9
PFO	R^2	0.9994	0.9998	0.9995	0.9746	0.9935	0.9998	0.9982	0.9988	0.9988
	X^2	0.0058	0.0019	0.0055	0.1848	0.0492	0.0017	0.0242	0.0163	0.0172
PSO	R^2	0.9998	0.9999	0.9998	0.9876	0.9977	0.9998	0.9990	0.9993	0.9995
	X^2	0.0020	0.0004	0.0025	0.0909	0.0177	0.0020	0.0129	0.0095	0.0073
DI	R^2	0.7535	0.7384	0.7394	0.9049	0.8221	0.7345	0.7592	0.7592	0.7635
	Chi^2	2.2569	2.4451	2.6378	0.7456	1.3775	2.1384	3.3027	3.3397	3.4471

(nanometer size), which promotes the diffusion of phosphate ions [66,69,121]. Thus, values higher than 20 mV keep the particles in suspension, maximizing the contact area for adsorption with a consequent increase in the diffusion of phosphate ions.

3.4. Adsorption isotherms

The studied models reported R^2 values close to unity (Table 7), with low values of X^2, ARE, HYBRID, and MPSD, which justifies that the models allow to adequately represent the phosphorus adsorption process in AA, NS-AH, and NCC (Fig. 3c).

The maximum phosphorus adsorption at the monolayer level (q_m), evaluated through the Langmuir model, was greater in AA (94.93 mg/g), following the order AA > NCC > NS-AH. This suggests that AA presents positively charged active sites on the surface or monolayer, allowing it to quickly become saturated with the phosphate forms of phosphorus. Although the ζ potential of the materials indicates an inverse order, that is, a greater net negative charge of the conglomerate of the materials, it must be understood that the adsorption evaluated through q_m allows us to know the adsorption behavior at the monolayer level [136,137].

Table 7
Model parameters of adsorption isotherms.

Model	Parameters	AA	NS-AH	NCC
Langmuir	q_m (mg/g)	94.93	70.92	92.45
	K_L (L/mg)	0.011	0.008	0.022
	R^2	0.99	0.98	1.00
	X^2	1.18	2.06	1.06
	ARE	13.42	23.69	10.17
	HYBRID	20.14	35.53	15.25
	MPSD	1.99	2.69	1.86
Freundlich	K_F ($mg^{1-1/n}/L^n$)	3.47	1.84	7.14
	$1/n$	0.57	0.60	0.46
	n	1.77	1.65	2.17
	R^2	0.97	0.94	0.96
	X^2	4.83	4.86	6.51
	ARE	32.68	43.71	31.63
	HYBRID	49.02	65.57	47.45
	MPSD	4.51	4.32	5.91
Redlich-Peterson	K_R (L/g)	0.91	0.40	1.91
	a_R (1/mg)	0.003	0.000	0.018
	g	1.20	2.23	1.03
	R^2	1.00	0.99	1.00
	X^2	0.79	0.56	0.98
	ARE	10.12	11.68	9.67
	HYBRID	20.24	23.35	19.33
	MPSD	2.07	1.49	2.12
Temkin	b_T (J/Mol)	135.35	184.80	129.42
	A_T (L/mg)	0.16	0.12	0.27
	R^2	0.98	0.96	1.00
	X^2	1.37	2.23	0.30
	ARE	21.95	33.89	7.54
	HYBRID	32.92	50.84	11.31
	MPSD	3.78	3.77	2.04
Dubinin Radushkevich	q_D (mg/g)	59.18	42.64	66.95
	k_D ($mMol^2/J^2$)	164.40	307.53	67.08
	R^2	0.95	0.98	0.94
	X^2	2.65	0.42	3.13
	ARE	25.04	21.92	25.33
	HYBRID	37.56	32.87	38.00
	MPSD	5.55	2.33	7.19

During the adsorption process, it was observed that the studied materials have low K_L values (Table 7), indicating that they have a high affinity and favorable adsorption of phosphorus at pH 8. With increasing adsorbate, the adsorption is more favorable, reporting lower separation factor (R_L) values (Fig. 3d), suggesting that the chemisorption process predominates in the adsorbent-adsorbate interaction.

The K_F parameter of the Freundlich model is related to the adsorption capacity or strength. It was found in the order NCC >> AA > NS-AH (Table 7). Values between 1.0 to 10.0 suggest moderate to high adsorption, although, for adsorbents of cellulosic origin used for the removal of organic contaminants, K_F is in the range of 0.1 to 5.0 indicating low to moderate removal capacity [43,138,139].

It was observed that the parameter n of the Freundlich molding followed the order NCC > AA > NS-AH, reporting values greater than 1.0 (Table 7), indicating that the adsorption process is favorable [140] and that the NCC and AA present surface highly heterogeneous with high affinity for phosphorus, being lower for NS-AH. This indicates that this material has fewer defects and available adsorption sites, which is reflected in the higher crystallinity index (90.90 %), resulting in lower phosphorus removal.

The K_R parameter of the Redlich-Peterson model allows to relate the adsorption strength of the adsorbents studied, establishing the order NCC > AA > NS-AH. Likewise, the values of a_R for the adsorbents were found to be close to zero, indicating that the materials have a high heterogeneity, which is related to g, which presented values greater than 1.0 [32,141].

The b_T parameter of the Temkin model reported high values for the adsorbents studied, indicating that the heterogeneity decreases and the energy distribution is less uniform in the NCC, AA, and NS-AH order. Values lower than 10 kJ/mol are characteristic of chemisorption processes with high heat of adsorption [142]. Likewise, it was observed that A_T is higher for NCC, indicating that this material has favorable adsorption with higher adsorption capacity. However, the values for AA, and NS-AH are not significantly different. A_T values between 0.1 and 1.0 L/g indicate moderate adsorption, which is characteristic of adsorption systems with cellulosic materials [35,137]. Similarly, for A_T > 0.01 mg L/mg, it is suggested that it dominates the chemisorption process [142]. These results confirm the results obtained with the Langmuir, Freundlich, and Redlich-Peterson models.

The theoretical adsorption capacity at the q_D monolayer level of the Dubinin-Radushkevich model reported values of 66.95 mg/g for NCC, suggesting moderate to high adsorption typical of porous materials that can be used at low temperatures [143,144]. The values found for k_D are typical of heterogeneous materials, with strong interactions between adsorbate and adsorbent, manifesting chemisorption processes [51,56,143].

On the other hand, the Gibbs free energy, calculated through the K_L parameter of the Langmuir model, considering a dilute P solution [36,145], indicated that the process is spontaneous (ΔG < 0) (Table 8), that

Table 8
Energy values during adsorption process.

Energy		AA	NS-AH	NCC
Gibbs free	ΔG (J/mol)	-26.83	-19.59	-52.48
Adsorption free	E (kJ/mol)	55.15	40.32	86.33

is, without the need for the addition of external energy for the P to adhere naturally to the adsorbent.

The adsorption free energy, calculated through the Dubinin Radushkevich model, indicated that the adsorption process is governed by chemisorption, since E > 8.0 kJ/mol (Table 8), that is, the interaction between P and the adsorbent is established by chemical bonds, which can lead to irreversible P adsorption [37,146].

Chemisorption processes allow the establishment of strong, irreversible interactions with high adsorption energy between phosphate ions and adsorbents. AA and NCC adsorbents modified with low-reactivity substances increase the active sites and surface area. Although this capacity could be limited in real conditions by competition from other adsorbents, suspended particles, and microorganisms could diffuse into the interstitial pores of the adsorbents studied. ZCP is a crucial indicator in the adsorption process, therefore controlling the pH and temperature of the process would allow improving the adsorption capacity. Copolymerization, doping or the addition of other materials to the adsorbents have been tested to provide higher affinity and phosphorus adsorption capacity [7,10,12,16,124,147]. Therefore, the adsorption process would tend to have a lyophobic behavior, that is, the adsorbent has a low affinity for water and a high affinity for phosphate [148,149]

However, the challenge remains to know the interactions with other particulate and suspended materials in wastewater treatment, which could reduce the phosphorus adsorption capacity of these materials, especially for AA and NCC. However, the use of these materials is highly advantageous because they come from natural sources whose activation has hardly required physical modification or the use of substances with low reactivity for the environment, making them promoters of the circular economy and sustainable development.

Another aspect to consider is the potential for regeneration and reuse after use in phosphorus removal. Regeneration methods involving chemical and thermal treatments and water washing offer specific advantages. Regeneration efficiency is usually high for porous materials such as cellulose and cation-exchange materials such as clay, reaching 80-95 % of initial capacity after the first regeneration; however, cellulose can be used for at least 6 cycles [103,150,151]. While those that exhibit covalent bonding with the adsorbent are usually less susceptible to reuse, this is the case with NS-AH. Although these experiments have not been carried out in the present study, the regenerative capacity of AA and NCC may be considerable due to the activation processes to which they have been subjected.

4. Conclusions

The materials studied, cellulose nanocrystals esterified with citric acid (NCC), activated clay (AA) with 1.0 M NaCl, and nostoc hydrocolloid (NS-AH), exhibit physical, chemical, thermal, and structural properties that allow the removal of phosphorus in the form of phosphate in aqueous media. The affinity for P was in the order of NCC > AA > NS-AH, this preference is mainly conditioned by the crystallinity index, particle size, zero charge point, ζ potential as well as the functional groups. The adsorption capacity at 120 min was up to 16.17, 13.45, and 9.25 mg P/g, with the removal of up to 89.44, 70.35, and 51.66 % P for NCC, AA, and NS-AH, respectively, which increased significantly in alkaline medium (pH 8), from a solution of 20 ppm P. The adsorption kinetics study showed a good fit for the PFO, PSO, and Intraparticle Diffusion models with high adsorption rates for AA and NCC in the first 20 min. Adsorption isotherms suggested that the adsorbents present heterogeneous surfaces with high porosity and govern chemisorption processes, with high affinity and favorable phosphorus adsorption at pH 8 in the order NCC > AA > NS-AH. The materials studied present good qualities to be used as phosphorus adsorbents in the form of phosphates in aqueous media. The materials studied obey chemisorption processes, with lyophobic behavior, with stable nanoparticle sizes, making them a potential alternative for use as adsorbents in the removal of phosphorus from wastewater.

CRediT authorship contribution statement

Aydeé Kari-Ferro: Writing – review & editing, Writing – original draft, Supervision, Project administration, Investigation, Funding acquisition, Formal analysis, Conceptualization. **Aydeé M. Solano-Reynoso:** Writing – original draft, Investigation, Conceptualization. **Celinda Alvarez-Arias:** Software, Methodology, Investigation, Formal analysis, Data curation. **Nora Gladis Echegaray-Peña:** Investigation, Data curation, Conceptualization. **David Choque-Quispe:** Writing – review & editing, Writing – original draft, Validation, Software, Methodology, Formal analysis, Conceptualization.

Declaration of competing interest

The authors declare that they have no known competing financial interests or personal relationships that could have appeared to influence the work reported in this paper.

Acknowledgements

The authors would like to thank the Vicerrectoría de Investigación de la Universidad Nacional Micaela Bastidas for funding the research. They also thank the Vicerrectoría de Investigación de la Universidad Nacional José María Arguedas in the context of Resolution N° 102-2022-CU-UNAMBA and Resolution N°191-2023-CO-UNAJMA.

Funding

This research was funded by Vicerrectorado de Investigación de la Universidad Nacional Micaela Bastidas, Abancay, Apurímac, Perú. Resolution N° 102-2022-CU-UNAMBA.

Data availability

Data will be made available on request.

References

[1] E.H. Khader, S.A. Muslim, N.M.C. Saady, N.S. Ali, I.K. Salih, T.J. Mohammed, T. M. Albayati, S. Zendehboudi, Recent advances in photocatalytic advanced oxidation processes for organic compound degradation: a review, Desalin. Water Treat. (2024) 100384.

[2] X. Chen, Y. Wang, Z. Bai, L. Ma, M. Strokal, C. Kroeze, X. Chen, F. Zhang, X. Shi, Mitigating phosphorus pollution from detergents in the surface waters of China, Sci. Total Environ. 804 (2022) 150125, https://doi.org/10.1016/j.scitotenv.2021.150125.

[3] Ahmad, S.Z.N.; Hamdan, R.; Mohamed, W.A.W.; Othman, N.; Zin, N.S.M.; Musa, S. Comparisons study of phosphate removal in unaerated and aerated high calcium steel slag filter system of different pH feed. 2017, 2017; p. 06018.

[4] Y. Wang, D. Sun, Phosphate removal from aqueous solutions on fly ash with medium calcium content, Korean J. Chem. Eng. 32 (2015) 1323–1326.

[5] J. Chuquimboques Marrero, J. Vergara Rojasa, J. Mendoza Bobadilla, Optimización de la remoción simultánea de nitrato, nitrito, amonio y fosfato de aguas residuales municipales, Revi. Soc. Quím. Perú 85 (2019) 85–96.

[6] T. Li, P. Zhou, Y. Ding, Q. Tang, S. Zhou, Y. Liu, Distribution characteristics and source analysis of nitrogen and phosphorus in different rivers in two water period: A case study of Pi River and Shiting River in the upper reaches of Tuo River in China, Int. J. Environ. Res. Public Health 19 (2022) 12433, https://doi.org/10.3390/ijerph191912433.

[7] S.K. Ramasahayam, L. Guzman, G. Gunawan, T. Viswanathan, A comprehensive review of phosphorus removal technologies and processes, J. Macromol. Sci. Part A 51 (2014) 538–545.

[8] Y. Li, X. Nan, D. Li, L. Wang, R. Xu, Q. Li, Advances in the treatment of phosphorus-containing wastewater, in: Proceedings of the Earth and Environmental Science 2021, 2021 012163.

[9] A. Masłoń, J. Czarnota, Efficiency of brick dust and powdered ceramsite in the phosphorus removal from wastewater, *J. Ecol. Eng.* (2020) 21.

[10] Y. Zheng, Y. Wan, Y. Zhang, J. Huang, Y. Yang, D.C.W. Tsang, H. Wang, H. Chen, B. Gao, Recovery of phosphorus from wastewater: A review based on current phosphorous removal technologies, Crit. Rev. Environ. Sci. Technol. 53 (2023) 1148–1172.

[11] J. Šarko, A. Mažeikienė, Investigation of sorbents for phosphorus removal, in: Proceedings of the Environmental Engineering. Proceedings of the International Conference on Environmental Engineering, ICEE, 2020, pp. 1–8, 2020.

[12] S. Gubernat, A. Masłoń, J. Czarnota, P. Koszelnik, Reactive materials in the removal of phosphorus compounds from wastewater—A review, Materials 13 (2020) 3377.

[13] C. Vohla, M. Kõiv, H.J. Bavor, F. Chazarenc, Ü. Mander, Filter materials for phosphorus removal from wastewater in treatment wetlands—A review, Ecol. Eng. 37 (2011) 70–89.

[14] N. Khalaf, J.J. Leahy, W. Kwapinski, Phosphorus recovery from hydrothermal carbonization of organic waste: a review, J. Chem. Technol. Biotechnol. 98 (2023) 2365–2377.

[15] D. Choque-Quispe, Y. Choque-Quispe, C.A. Ligarda-Samanez, D.E. Peralta-Guevara, A.M. Solano-Reynoso, B.S. Ramos-Pacheco, F. Taipe-Pardo, E. L. Martínez-Huamán, J.P. Aguirre Landa, H.W. Agreda Cerna, et al., Effect of the addition of corn husk cellulose nanocrystals in the development of a novel edible film, Nanomaterials 12 (2022), https://doi.org/10.3390/nano12193421.

[16] X. Chen, L. Wu, F. Liu, P. Luo, X. Zhuang, J. Wu, Z. Zhu, S. Xu, G. Xie, Performance and mechanisms of thermally treated bentonite for enhanced phosphate removal from wastewater, *Environ. Sci. Pollut. Res.* 25 (2018) 15980–15989.

[17] A.L. Ciosek, G.K. Luk, M. Warner, R.A. Warner, An Innovative Design of a Clay-Zeolite Medium for the Adsorption of Total Phosphorus from Wastewater, Water Environ. Res. 88 (2016) 131–142.

[18] H.J. Sun, S.H. Yang, Y.B. Cui, Shell powder for strengthening phosphate removal efficiency in wastewater treatment, Adv. Mat. Res. 781 (2013) 2138–2141.

[19] A.A. Owodunni, S. Ismail, S.B. Kurniawan, A. Ahmad, M.F. Imron, S.R. S. Abdullah, A review on revolutionary technique for phosphate removal in wastewater using green coagulant, J. Water. Process. Eng. 52 (2023) 103573.

[20] B.N.S. Al-dhawi, S.R.M. Kutty, L. Baloo, N.M.Y. Almahbashi, A.A.S. Ghaleb, A. H. Jagaba, V. Kumar, A.A.H. Saeed, Phosphorus removal from synthetic wastewater by using palm oil clinker as media in continuous activated sludge. Sustainability challenges and delivering practical engineering solutions: resources, materials, energy, and buildings, Springer, 2023, pp. 41–44.

[21] V.O. Shikuku, N.W. Masinde, Machine learning applications in adsorption of water pollutants. Artificial Intelligence Applications in Water Treatment and Water Resource Management, IGI Global, 2023, pp. 1–30.

[22] C.A. Ligarda-Samanez, D. Choque-Quispe, H. Palomino-Rincón, B.S. Ramos-Pacheco, E. Moscoso-Moscoso, M.L. Huamán-Carrión, D.E. Peralta-Guevara, M. E. Obregón-Yupanqui, J. Aroni-Huamán, E.Y. Bravo-Franco, et al., Modified Polymeric Biosorbents from Rumex acetosella for the Removal of Heavy Metals in Wastewater, Polymers (Basel) 14 (2022), https://doi.org/10.3390/polym14112191.

[23] S.M. Abegunde, K.S. Idowu, O.M. Adejuwon, T. Adeyemi-Adejolu, A review on the influence of chemical modification on the performance of adsorbents, *Resour. Environ. Sustain.* 1 (2020) 100001.

[24] L. Deng, Z. Shi, Synthesis and characterization of a novel Mg–Al hydrotalcite-loaded kaolin clay and its adsorption properties for phosphate in aqueous solution, J. Alloys. Compd. 637 (2015) 188–196.

[25] A.Q. Selim, L. Sellaoui, M. Mobarak, Statistical physics modeling of phosphate adsorption onto chemically modified carbonaceous clay, J. Mol. Liq. 279 (2019) 94–107.

[26] A. Valverde, A. Cabrera-Codony, M. Calvo-Schwarzwalder, T.G. Myers, Investigating the impact of adsorbent particle size on column adsorption kinetics through a mathematical model, Int. J. Heat. Mass Transf. 218 (2024) 124724.

[27] L. Ding, C. Wu, H. Deng, X. Zhang, Adsorptive characteristics of phosphate from aqueous solutions by MIEX resin, J. Colloid. Interface Sci. 376 (2012) 224–232.

[28] J. Wang, X. Guo, Rethinking of the intraparticle diffusion adsorption kinetics model: Interpretation, solving methods and applications, Chemosphere 309 (2022) 136732.

[29] Tighadouini, S.; Radi, S.; Roby, O.; Hammoudan, I.; Saddik, R.; Garcia, Y.; Almarhoon, Z.M.; Mabkhot, Y.N.J.R.a. Kinetics, thermodynamics, equilibrium, surface modelling, and atomic absorption analysis of selective Cu (ii) removal from aqueous solutions and rivers water using silica-2-(pyridin-2-ylmethoxy) ethan-1-ol hybrid material. 2022, 12, 611-625.

[30] D. Choque-Quispe, B.S. Ramos-Pacheco, C.A. Ligarda-Samanez, G.I. Barboza-Palomino, A. Kari-Ferro, F. Taipe-Pardo, Y. Choque-Quispe, Heavy metal removal by biopolymers-based formulations with native potato starch/nopal mucilage, Rev. Fac. Ing. Univ. Antioq. (2022) 44–50.

[31] W.J. Weber Jr, J.C Morris, Kinetics of adsorption on carbon from solution, J. Sanit. Eng. Div. 89 (1963) 31–59.

[32] K. Stepova, L. Sysa, R. Konanets, Nonlinear fitting of iron sorption on bentonite to theoretical isotherm models, Phys. Chem. Solid State 23 (2022) 270–276.

[33] E.O. Oyelude, J.A.M. Awudza, S.K. Twumasi, Removal of malachite green from aqueous solution using pulverized teak leaf litter: equilibrium, kinetic and thermodynamic studies, Chem. Cent. J. 12 (2018) 81, https://doi.org/10.1186/s13065-018-0448-8.

[34] M. Šuránek, Z. Melichová, V. Kureková, L. Kljajević, S. Nenadović, Removal of nickel from aqueous solutions by natural bentonites from slovakia, Materials 14 (2021), https://doi.org/10.3390/ma14020282.

[35] K.H. Chu, Revisiting the Temkin isotherm: dimensional inconsistency and approximate forms, Ind. Eng. Chem. Res. 60 (2021) 13140–13147.

[36] R. Ezzati, A new insight into the surface adsorption in the solution phase: a modification of the langmuir isotherm, Water Environ. Res. 96 (2024) e11019.

[37] A. Mudhoo, C.U. Pittman Jr, The Dubinin-Radushkevich Models: Dissecting the ps/p to cs/ce Replacement in Solid-aqueous Interfacial Adsorption and Tracking the Validity of E= 8 kJ mol–1 for Assigning Sorption Type, Chem. Eng. Res. Des. (2023).

[38] E. Moscoso-Moscoso, C.A. Ligarda-Samanez, D. Choque-Quispe, M.L. Huamán-Carrión, J.C. Arévalo-Quijano, G. De la Cruz, R. Luciano-Alipio, W.C. Calsina Ponce, R. Sucari-León, U.R. Quispe-Quezada, Preliminary assessment of tara gum as a wall material: physicochemical, structural, thermal, and rheological analyses of different drying methods, Polym. (Basel) 16 (2024) 838.

[39] K. Dome, E. Podgorbunskikh, A. Bychkov, O. Lomovsky, Changes in the crystallinity degree of starch having different types of crystal structure after mechanical pretreatment, Polym. (Basel) 12 (2020) 641.

[40] A. Monshi, M.R. Foroughi, M.R. Monshi, Modified Scherrer equation to estimate more accurately nano-crystallite size using XRD, World J. Nano Sci. Eng. 2 (2012) 154–160.

[41] D. Choque-Quispe, F.H.O. Gonzales, M.V. Carranza-Oropeza, A.M. Solano-Reynoso, C.A. Ligarda-Samanez, W. Palomino-Ríncón, K. Choque-Quispe, M. J. Torres-Calla, Physicochemical and technofunctional properties of high Andean native potato starch, J. Agric. Food Res. 15 (2024) 100955.

[42] K. Rani, T. Gomathi, K. Vijayalakshmi, M. Saranya, P.N. Sudha, Banana fiber cellulose nano crystals grafted with butyl acrylate for heavy metal lead (II) removal, Int. J. Biol. Macromol. 131 (2019) 461–472, https://doi.org/10.1016/j.ijbiomac.2019.03.064.

[43] A.S. Singha, A. Guleria, Chemical modification of cellulosic biopolymer and its use in removal of heavy metal ions from wastewater, Int. J. Biol. Macromol. 67 (2014) 409–417, https://doi.org/10.1016/j.ijbiomac.2014.03.046.

[44] Y.S. Murillo, L. Giraldo, J.C. Moreno, Determination of the 2, 4-dinitrofenol adsorption kinetic on bovine bone char by UV-Vis spectrophotometry, Rev. Colomb. Quím. 40 (2011) 91–103.

[45] K. Rajeshwari, S. Latha, T. Gomathi, K. Sangeetha, P.N. Sudha, Adsorption of heavy metal Cr (VI) By a ternary biopolymer blend, Mater. Today Proc. 5 (2018) 14628–14638, https://doi.org/10.1016/j.matpr.2018.03.054.

[46] S. Lagergren, About the theory of so-called adsorption of soluble substances, Vetenskapsakad. Handl. 24 (1898).

[47] W. Plazinski, W. Rudzinski, A. Plazinska, Theoretical models of sorption kinetics including a surface reaction mechanism: a review, Adv. Colloid. Interface Sci. 152 (2009) 2–13.

[48] J. Wang, X. Guo, Adsorption kinetic models: Physical meanings, applications, and solving methods, J. Hazard. Mater. 390 (2020) 122156.

[49] Y.S. Ho, G. McKay, A comparison of chemisorption kinetic models applied to pollutant removal on various sorbents, Process. saf. Environ. Prot. 76 (1998) 332–340.

[50] J.C. Igwe, A review of potentially low cost sorbents for heavy metal removal and recovery, Terrestrial Aquatic Environ. Toxicol. 1 (2007) 60–69.

[51] P. Ramachandran, R. Vairamuthu, S. Ponnusamy, Adsorption isotherms, kinetics, thermodynamics and desorption studies of reactive Orange 16 on activated carbon derived from Ananas comosus (L.) carbon, J. Eng. Appl. Sci. 6 (2011) 15–26.

[52] M.K. Seliem, S. Komarneni, T. Byrne, F.S. Cannon, M.G. Shahien, A.A. Khalil, I. M. Abd El-Gaid, Removal of nitrate by synthetic organosilicas and organoclay: Kinetic and isotherm studies, Sep. Purif. Technol. 110 (2013) 181–187, https://doi.org/10.1016/j.seppur.2013.03.023.

[53] O. Redlich, D.L. Peterson, A useful adsorption isotherm, J. Phys. Chem. 63 (1959), 1024-1024.

[54] M. Vadi, M. Salmanpour, S. Bolqar, Investigation of Langmuir, Freundlich and Temkin isotherms of Letrozole by single-wall carbon nanotube and multi-wall carbon nanotube, Res. J. Pharm. Biol. Chem. Sci. 5 (2014) 52–56.

[55] V.O. Shikuku, T. Mishra, Adsorption isotherm modeling for methylene blue removal onto magnetic kaolinite clay: a comparison of two-parameter isotherms, Appl. Water. Sci. 11 (2021) 103.

[56] T.V.N. Padmesh, K. Vijayaraghavan, G. Sekaran, M. Velan, Application of two- and three-parameter isotherm models: biosorption of acid red 88 onto azolla microphylla, Bioremediat. J. 10 (2006) 37–44, https://doi.org/10.1080/10889860600842746.

[57] I. Emiola, R. Adem, Comparison of minimization methods for rosenbrock functions, in: Proceedings of the 2021 29th Mediterranean Conference on Control and Automation (MED), 22-25 June 2021, 2021, pp. 837–842.

[58] S.J. Allen, G. McKay, J.F. Porter, Adsorption isotherm models for basic dye adsorption by peat in single and binary component systems, J. Colloid. Interface Sci. 280 (2004) 322–333.

[59] G.F. El-Said, M.M. El-Sadaawy, M.A. Aly-Eldeen, Adsorption isotherms and kinetic studies for the defluoridation from aqueous solution using eco-friendly raw marine green algae, Ulva lactuca, Environ. Monit. Assess. 190 (2017) 14, https://doi.org/10.1007/s10661-017-6392-6.

[60] L.T. Popoola, A.S. Yusuff, O.A. Adesina, M.A. Lala, Brilliant green dye sorption onto snail shell-rice husk: statistical and error function models as parametric isotherm predictors, J. Environ. Sci. Technol. 12 (2019) 65–80.

[61] F. Zhang, X. Tang, Y. Huang, A.A. Keller, J. Lan, Competitive removal of Pb2+ and malachite green from water by magnetic phosphate nanocomposites, Water. Res. 150 (2019) 442–451, https://doi.org/10.1016/j.watres.2018.11.057.

[62] M. Kosmulski, The pH dependent surface charging and points of zero charge. IX. Update, Adv. Colloid. Interface Sci. 296 (2021) 102519.

[63] A.H. Zyoud, A. Zubi, S.H. Zyoud, M.H. Hilal, S. Zyoud, N. Qamhieh, A. Hajamohideen, H.S. Hilal, Kaolin-supported ZnO nanoparticle catalysts in self-sensitized tetracycline photodegradation: Zero-point charge and pH effects, Appl. Clay. Sci. 182 (2019) 105294, https://doi.org/10.1016/j.clay.2019.105294.

[64] J. Kollannur Nikhil, N. Arnepalli Dali, Methodology for determining point of zero salt effect of clays in terms of surface charge properties, J. Mater. Civ. Eng. 31 (2019) 04019286, https://doi.org/10.1061/(ASCE)MT.1943-5533.0002947.

[65] R. Kecili, C.M. Hussain, Mechanism of adsorption on nanomaterials. Nanomaterials in chromatography, Elsevier, 2018, pp. 89–115.

[66] R. Bushra, A. Ahmed, M Shahadat, Mechanism of Adsorption on Nanomaterials, in: C.M. Hussain, B. Kharisov, C.M. Hussain, B. Kharisov (Eds.), Advanced Environmental Analysis: Applications of Nanomaterials, Volume 1, The Royal Society of Chemistry, 2016, p. 0.

[67] S. Skoglund, J. Hedberg, E. Yunda, A. Godymchuk, E. Blomberg, Odnevall Wallinder, I. Difficulties and flaws in performing accurate determinations of zeta potentials of metal nanoparticles in complex solutions—Four case studies, PLoS One 12 (2017) e0181735.

[68] S. Kamble, S. Agrawal, S. Cherumukkil, V. Sharma, R.V. Jasra, P. Munshi, Revisiting zeta potential, the key feature of interfacial phenomena, with applications and recent advancements, ChemistrySelect 7 (2022) e202103084.

[69] Z. Zhang, A new method for estimating zeta potential of carboxylic acids' functionalised particles, Mol. Phys. (2023) e2260014.

[70] V.D. Kotlyar, A.V. Kozlov, A.V. Kotlyar, Granulometric composition particulars of lithoidal clay raw material as determined by laser diffraction, Glass Ceram. 74 (2017) 131–136.

[71] N.A. Mamat Razali, N. Azraaie, N.A.M. Zainul Abidin, N.A. Ibrahim, F. Abdul Aziz, S.A. Rahman, Preparation and XRD analysis of cellulose from merbau (Intsia bijuga), Adv. Mat. Res. 895 (2014) 151–154.

[72] W. Yao, Y. Weng, J.M. Catchmark, Improved cellulose X-ray diffraction analysis using Fourier series modeling, Cellulose 27 (2020) 5563–5579.

[73] S. Park, J.O. Baker, M.E. Himmel, P.A. Parilla, D.K. Johnson, Cellulose crystallinity index: measurement techniques and their impact on interpreting cellulase performance, Biotechnol. Biofuels. 3 (2010) 1–10.

[74] C. Mutungi, F. Rost, C. Onyango, D. Jaros, H. Rohm, Crystallinity, thermal and morphological characteristics of resistant starch type III produced by hydrothermal treatment of debranched cassava starch, Starch-Stärke 61 (2009) 634–645.

[75] E.E. Santiso, Understanding the effect of adsorption on activated processes using molecular theory and simulation, Mol. Simul. 40 (2014) 664–677.

[76] Y. Zhao, B. Li, C. Li, Y. Xu, Y. Luo, D. Liang, C. Huang, Comprehensive review of polysaccharide-based materials in edible packaging: A sustainable approach, Foods 10 (2021) 1845.

[77] S.S.N. Chakravartula, M. Soccio, N. Lotti, F. Balestra, M. Dalla Rosa, V. Siracusa, Characterization of composite edible films based on pectin/alginate/whey protein concentrate, Materials 12 (2019) 2454.

[78] Y. Chen, C. Zou, M. Mastalerz, S. Hu, C. Gasaway, X. Tao, Applications of micro-fourier transform infrared spectroscopy (FTIR) in the geological sciences—a review, Int. J. Mol. Sci. 16 (2015) 30223–30250.

[79] M. Djebbar, F. Djafri, M. Bouchekara, A. Djafri, Adsorption of phenol on natural clay, Appl. Water. Sci. 2 (2012) 77–86.

[80] S. Rodriguez, F.G. Torres, D. López, Preparation and characterization of polysaccharide films from the cyanobacteria Nostoc commune, Polym. Renew. Resour. 8 (2017) 133–150.

[81] V. Sessini, M.P. Arrieta, J.M. Kenny, L. Peponi, Processing of edible films based on nanoreinforced gelatinized starch, Polym. Degrad. Stab. 132 (2016) 157–168, https://doi.org/10.1016/j.polymdegradstab.2016.02.026.

[82] N. Hamrun, B. Talib, M. Ruslin, H. Pangeran, M. Hatta, E. Marlina, A.S.H. Yusuf, T. Saito, K.-L. Ou, A promising potential of brown algae Sargassum polycystum as irreversible hydrocolloid impression material, Mar. Drugs 20 (2022) 55.

[83] K. Aftab, S. Hameed, H. Umbreen, S. Ali, M. Rizwan, S. Alkahtani, M.M. Abdel-Daim, Physicochemical and functional potential of hydrocolloids extracted from some Solanaceae plants, J. Chem. 2020 (2020) 1–9.

[84] Y. Xi, Z. Ding, H. He, R.L. Frost, Infrared spectroscopy of organoclays synthesized with the surfactant octadecyltrimethylammonium bromide, Spectrochimica. Acta Part A: Mol. Biomol. Spectrosc. 61 (2005) 515–525.

[85] H.A. Patel, R.S. Somani, H.C. Bajaj, R.V. Jasra, Nanoclays for polymer nanocomposites, paints, inks, greases and cosmetics formulations, drug delivery vehicle and waste water treatment, Bull. Mater. Sci. 29 (2006) 133–145.

[86] S. Bureau, D. Cozzolino, C.J. Clark, Contributions of Fourier-transform mid infrared (FT-MIR) spectroscopy to the study of fruit and vegetables: A review, Postharvest Biol. Technol. 148 (2019) 1–14.

[87] N. Sebeia, M. Jabli, A. Ghith, Y. Elghoul, F.M. Alminderej, Production of cellulose from Aegagropila Linnaei macro-algae: Chemical modification, characterization and application for the bio-sorptionof cationic and anionic dyes from water, Int. J. Biol. Macromol. 135 (2019) 152–162.

[88] L.A. Al Juhaiman, D.A. Al-Enezi, W.K Mekhamer, Preparation and characterization of polystyrene/organoclay nanocomposites from raw clay, Dig. J. Nanomater. Biostruct 11 (2016) 105–114.

[89] S. Louati, S. Baklouti, B. Samet, Geopolymers based on phosphoric acid and illito-kaolinitic clay, *Adv. Mater. Sci. Eng.* 2016 (2016).

[90] D. Choque-Quispe, A. Mojo-Quisani, C.A. Ligarda-Samanez, M. Calla-Florez, B. S. Ramos-Pacheco, L.M. Zamalloa-Puma, D.E. Peralta-Guevara, A.M. Solano-Reynoso, Y. Choque-Quispe, A. Zamalloa-Puma, Preliminary characterization of a spray-dried hydrocolloid from a high Andean algae (Nostoc sphaericum), Foods 11 (2022) 1640.

[91] X. Huang, D.Y. Zemlyanov, S. Diaz-Amaya, M. Salehi, L. Stanciu, A.J. Whelton, Competitive heavy metal adsorption onto new and aged polyethylene under various drinking water conditions, J. Hazard. Mater. 385 (2020) 121585.

[92] H.-W. Ma, H.-C. Shih, M.-I. Liao, Circular economy and new research directions in sustainability, Pursuing Sustainability: OR/MS Applications in Sustainable Design, Manufacturing, Logistics, and Resource Management (2021) 141–168.

[93] A. Elgamouz, N. Tijani, I. Shehadi, K. Hasan, M.A.-F. Kawam, Characterization of the firing behaviour of an illite-kaolinite clay mineral and its potential use as membrane support, Heliyon 5 (2019).

[94] I.F. Macías-Quiroga, G.I. Giraldo-Gómez, N.R. Sanabria-González, Characterization of Colombian clay and its potential use as adsorbent, Sci.World J. 2018 (2018).

[95] O. Ombaka, Characterization and classification of clay minerals for potential applications in Rugi Ward, Kenya, Afr. J. Environ. Sci. Tech. 10 (2016) 415–431.

[96] U.-J. Kim, S.H. Eom, M. Wada, Thermal decomposition of native cellulose: influence on crystallite size, Polym. Degrad. Stab. 95 (2010) 778–781.

[97] T.M. Albayati, S.M. Alardhi, A.H. Khalbas, Z.J. Humdi, N.S. Ali, I.K. Salih, N.M. C. Saady, S. Zendehboudi, M.A. Abdulrahman, Comprehensive review of mesoporous silica nanoparticles: drug loading, release, and applications as hemostatic agents, ChemistrySelect. 9 (2024) e202400450.

[98] J. Jung, M. Choi, A.K.R. Police, J. Lee, S. Bae, Removal of phosphorus by ferric ion-rich solutions prepared using various Fe (III)-containing minerals, Water (Basel) 14 (2022) 3765.

[99] X. Jia, T. Yin, Y. Wang, S. Zhou, X. Zhao, W. Chen, G. Hu, Porous honeycomb cork biochar for efficient and highly selective removal of phosphorus from wastewater, Biochar 5 (2023) 84.

[100] F. Hu, M. Wang, X. Peng, F. Qiu, T. Zhang, H. Dai, Z. Liu, Z. Cao, High-efficient adsorption of phosphates from water by hierarchical CuAl/biomass carbon fiber layered double hydroxide, Coll. Surf. A Physicochem. Eng. Aspects 555 (2018) 314–323.

[101] Q. Cui, G. Jiao, J. Zheng, T. Wang, G. Wu, G. Li, Synthesis of a novel magnetic Caragana korshinskii biochar/Mg–Al layered double hydroxide composite and its strong adsorption of phosphate in aqueous solutions, RSC. Adv. 9 (2019) 18641–18651.

[102] K.-W. Jung, S. Lee, Y.J. Lee, Synthesis of novel magnesium ferrite (MgFe2O4)/biochar magnetic composites and its adsorption behavior for phosphate in aqueous solutions, Bioresour. Technol. 245 (2017) 751–759.

[103] E. Shumiye, T.T. Nadew, T.S. Tedla, B. Getiye, D.A. Mengie, A.G. Ayalew, Preparation of an activated adsorbent from water treatment plant sludge for phosphate removal from wastewater: optimization, characterization, isotherm, and kinetics studies, J. Water. Sanit. Hyg. Dev. 14 (2024) 122–143.

[104] A.F. Santos, D.V. Lopes, P. Alvarenga, L.M. Gando-Ferreira, M.J. Quina, Phosphorus removal from urban wastewater through adsorption using biogenic calcium carbonate, J. Environ. Manage 351 (2024) 119875.

[105] P.D. Ramirez, C. Lee, R. Fedderwitz, A.R. Clavijo, D.P.P. Barbosa, M. Julliot, J. Vaz-Ramos, D. Begin, S. Le Calvé, A. Zaloszyc, Phosphate capture enhancement using designed iron oxide-based nanostructures, Nanomaterials 13 (2023) 587.

[106] H. Yin, Y. Yun, Y. Zhang, C. Fan, Phosphate removal from wastewaters by a naturally occurring, calcium-rich sepiolite, J. Hazard. Mater. 198 (2011) 362–369.

[107] M. Xanthopoulou, D. Giliopoulos, N. Tzollas, K.S. Triantafyllidis, M. Kostoglou, I. A. Katsoyiannis, Phosphate removal using polyethylenimine functionalized silica-based materials, Sustainability 13 (2021) 1502.

[108] X. Cui, A. Ozaki, T.-A. Asoh, H. Uyama, Cellulose modified by citric acid reinforced Poly (lactic acid) resin as fillers, Polym. Degrad. Stab. 175 (2020) 109118.

[109] D. Choque-Quispe, Y. Choque-Quispe, C.A. Ligarda-Samanez, D.E. Peralta-Guevara, A.M. Solano-Reynoso, B.S. Ramos-Pacheco, F. Taipe-Pardo, E. L. Martínez-Huamán, J.P. Aguirre Landa, H.W. Agreda Cerna, Effect of the addition of corn husk cellulose nanocrystals in the development of a novel edible film, Nanomaterials 12 (2022) 3421.

[110] A.D. Macheca, A.B. Mapossa, A.J. Cumbane, A.E. Sulemane, S.M. Tichapondwa, Development and characterization of Na2CO3-activated mozambican bentonite: Prediction of optimal activation conditions using statistical design modeling, Minerals 12 (2022) 1116.

[111] K.G. Bhattacharyya, S. Sen Gupta, Influence of acid activation of kaolinite and montmorillonite on adsorptive removal of Cd (II) from water, Ind. Eng. Chem. Res. 46 (2007) 3734–3742.

[112] A. Nayak, B. Bhushan, V. Gupta, P. Sharma, Chemically activated carbon from lignocellulosic wastes for heavy metal wastewater remediation: Effect of activation conditions, J. Colloid. Interface Sci. 493 (2017) 228–240.

[113] E.B. Ly, F. Brouillette, Understanding interactions between cellulose and phosphate esters in papermaking, *Am. J. Mater. Sci.* 3 (2013) 19–23.

[114] L. Wang, J. Wang, C. He, W. Lyu, W. Zhang, W. Yan, L. Yang, Development of rare earth element doped magnetic biochars with enhanced phosphate adsorption performance, Colloids Surf. A Physicochem. Eng. Aspects 561 (2019) 236–243.

[115] Q. Zhang, J. Teng, G. Zou, Q. Peng, Q. Du, T. Jiao, J. Xiang, Efficient phosphate sequestration for water purification by unique sandwich-like MXene/magnetic iron oxide nanocomposites, Nanoscale 8 (2016) 7085–7093.

[116] L.-g. Yan, K. Yang, R.-r. Shan, T. Yan, J. Wei, S.-j. Yu, H.-q. Yu, B. Du, Kinetic, isotherm and thermodynamic investigations of phosphate adsorption onto core–shell Fe3O4@ LDHs composites with easy magnetic separation assistance, J. Colloid. Interface Sci. 448 (2015) 508–516.

[117] M. Guessous, A. Rich, S. Mountadar, M. Siniti, M. Mountadar, Treatment of an industrial wastewater for phosphorus and fluoride recovery by a process coupling block freeze concentration and precipitation, J. Cryst. Growth 619 (2023) 127335.

[118] L. Bing, S. Jiancheng, C. Mengjun, Z. Xiangfei, L. Renlong, Y. Yong, A new basic burning raw material for simultaneous stabilization/solidification of PO43−-P and F− in phosphogypsum, Ecotoxicol. Environ. Saf. 252 (2023) 114582.
[119] T. Li, X. Su, X. Yu, H. Song, Y. Zhu, Y.La Zhang, OH) 3-modified magnetic pineapple biochar as novel adsorbents for efficient phosphate removal, Bioresour. Technol. 263 (2018) 207–213.
[120] J. Yang, B. Hou, J. Wang, B. Tian, J. Bi, N. Wang, X. Li, X. Huang, Nanomaterials for the removal of heavy metals from wastewater, Nanomaterials 9 (2019) 424.
[121] C. Wang, K. Huang, L. Mao, X. Liang, Z. Wang, Incorporation of La/UiO66-NH2 into cellulose fiber for efficient and selective phosphate adsorption, J. Environ. Chem. Eng. 12 (2024) 112257.
[122] Y. Zhou, J. Lu, Y. Zhou, Y. Liu, Recent advances for dyes removal using novel adsorbents: A review, Environ. Pollut. 252 (2019) 352–365, https://doi.org/10.1016/j.envpol.2019.05.072.
[123] L. Largitte, R. Pasquier, A review of the kinetics adsorption models and their application to the adsorption of lead by an activated carbon, Chem. Eng. Res. Des. 109 (2016) 495–504, https://doi.org/10.1016/j.cherd.2016.02.006.
[124] S.P. Moussavi, A. Kadier, N.S. Zaidi, P.T.P. Aryanti, F.A. Nugroho, J. Wang, P.-C. Ma, Removal of phosphorus from aqueous solution using multi-wall carbon nanotube (MWCNT) as adsorbent: Kinetics and isotherms, Fuller. Nanotub. Car. N 30 (2022) 589–595.
[125] V. Kokol, V. Vivod, Cation-exchange performance of a citric-acid esterified cellulose nanofibrous membrane for highly-selective proteins' permeability and adsorption capacity, Carbohydr. Polym. 318 (2023) 121134.
[126] A. Kausar, S.T. Zohra, S. Ijaz, M. Iqbal, J. Iqbal, I. Bibi, S. Nouren, N. El Messaoudi, A. Nazir, Cellulose-based materials and their adsorptive removal efficiency for dyes: a review, Int. J. Biol. Macromol. 224 (2023) 1337–1355.
[127] A.K. Dhar, H.A. Himu, M. Bhattacharjee, M.G. Mostufa, F. Parvin, Insights on applications of bentonite clays for the removal of dyes and heavy metals from wastewater: a review, Environ. Sci. Pollu. Res. 30 (2023) 5440–5474.
[128] A.A. Ayalew, A critical review on clay-based nanocomposite particles for application of wastewater treatment, Water Sci.Technol. 85 (2022) 3002–3022.
[129] H. Han, M.K. Rafiq, T. Zhou, R. Xu, O. Mašek, X. Li, A critical review of clay-based composites with enhanced adsorption performance for metal and organic pollutants, J. Hazard. Mater. 369 (2019) 780–796.
[130] S. Roy, R. Priyadarshi, Ł. Łopusiewicz, D. Biswas, V. Chandel, J.-W. Rhim, Recent progress in pectin extraction, characterization, and pectin-based films for active food packaging applications: A review, Int. J. Biol. Macromol. (2023) 124248.
[131] S. Basak, U.S. Annapure, Trends in "green" and novel methods of pectin modification-A review, Carbohydr. Polym. 278 (2022) 118967.
[132] M. Jiang, Y. Yang, T. Lei, Z. Ye, S. Huang, X. Fu, P. Liu, H. Li, Removal of phosphate by a novel activated sewage sludge biochar: Equilibrium, kinetic and mechanism studies, Appl. Energy Combust. Sci. 9 (2022) 100056.
[133] R.E. Mesmer, C.F. Baes, Phosphoric acid dissociation equilibria in aqueous solutions to 300 C, J. Solution. Chem. 3 (1974) 307–322.
[134] M. Chesneau, Applications du Carbone: Les Materiaux Carbones Actives. Carbone Dans Tous Ses Etats, Routledge, 2023, pp. 535–549.
[135] K. Taira, D. McInnes, L. Zhang, How many data points and how large an R-squared value is essential for Arrhenius plots? J. Catal. 419 (2023) 26–36.
[136] A. Hashem, A. Al-Anwar, N.M. Nagy, D.M. Hussein, S. Eisa, Isotherms and kinetic studies on adsorption of Hg (II) ions onto Ziziphus spina-christi L. from aqueous solutions, Green Process. Synth. 5 (2016) 213–224.
[137] F. Shojaeipoor, D. Elhamifar, R. Moshkelgosha, B. Masoumia, Removal of Pb (II) and Co (II) ions from aqueous solution and industrial wastewater using ILNO-NH2: Kinetic, isotherm and thermodynamic studies, J. Taiwan. Inst. Chem. Eng. 67 (2016) 166–173.
[138] H. Haroon, S.M.H. Gardazi, T.A. Butt, A. Pervez, Q. Mahmood, M. Bilal, Novel lignocellulosic wastes for comparative adsorption of Cr (VI): equilibrium kinetics and thermodynamic studies, Pol. J. Chem. Technol. 19 (2017) 6–15.
[139] S. Kokate, K. Parasuraman, H. Prakash, Adsorptive removal of lead ion from water using banana stem scutcher generated in fiber extraction process, Results. Eng. 14 (2022) 100439, https://doi.org/10.1016/j.rineng.2022.100439.
[140] M. Šuránek, Z. Melichová, V. Kureková, L. Kljajević, S. Nenadović, Removal of nickel from aqueous solutions by natural bentonites from slovakia, Materials 14 (2021) 282.
[141] H.N. Tran, E.C. Lima, R.-S. Juang, J.-C. Bollinger, H.-P. Chao, Thermodynamic parameters of liquid–phase adsorption process calculated from different equilibrium constants related to adsorption isotherms: A comparison study, J. Environ. Chem. Eng. 9 (2021) 106674.
[142] S. Seyfi, A.R. Azadmehr, A. Maghsoudi, Comparative and competitive adsorption of Cu (II) and Cd (II) using scoria: Equilibrium, kinetic and thermodynamic studies, Chem. Res. Chin. Univ. 33 (2017) 471–478.
[143] S. Shimizu, N. Matubayasi, Adsorbate-adsorbate interactions on microporous materials, Microp. Mesoporous Mater. 323 (2021) 111254.
[144] A.U. Štefanko, D. Leszczynska, Evaluation of Cd 2+, Cu 2+, Pb 2+, and Zn 2+ removal by cow manure and corn stover biochar with the emphasis on the solubility-normalized dubinin–radushkevich approach for the computation of the adsorption potential (ε), J. Environ. Eng. 147 (2021) 04021069.
[145] Y. Liu, Is the free energy change of adsorption correctly calculated? J. Chem. Eng. Data 54 (2009) 1981–1985.
[146] J. Devémy, A. Dequidt, P. Malfreyt, A consistent thermodynamic characterization of the adsorption process through the calculation of free energy contributions, The J. Phy. Chem. B 127 (2023) 5360–5370.
[147] S. Gubernat, A. Masłoń, J. Czarnota, P. Koszelnik, Phosphorus removal from wastewater using marl and travertine and their thermal modifications, Desalin. Water Treat. 275 (2022) 35–46.
[148] Y.A. Abd Al-Khodor, T.M Albayati, Employing sodium hydroxide in desulfurization of the actual heavy crude oil: Theoretical optimization and experimental evaluation, Process Saf. Environ. Prot. 136 (2020) 334–342.
[149] Shchukin, E.D.; Amelina, E.A.; Izmailova, V.N. The Lyophilic Structure-Mechanical Barrier as a Factor of Dispersion Strong Stabilization. 2003; pp. 81-90.
[150] B. Rezai, E. Allahkarami, Desorption/regeneration of adsorbents and their performance. Sustainable Technologies for Remediation of Emerging Pollutants from Aqueous Environment, Elsevier, 2024, pp. 263–283.
[151] M. Shahadat, S. Isamil, Regeneration performance of clay-based adsorbents for the removal of industrial dyes: a review, RSC Adv. 8 (2018) 24571–24587.